Study of the decay $\psi(3686) \to \Sigma^0\bar{\Sigma}^0\phi$

M. Ablikim *et al.*[*]
(BESIII Collaboration)

(Received 10 December 2024; accepted 24 January 2025; published 26 March 2025)

Using $(27.12 \pm 0.14) \times 10^8$ $\psi(3686)$ events collected with the BESIII detector operating at the BEPCII collider, we have observed the decay $\psi(3686) \to \Sigma^0\bar{\Sigma}^0\phi$ for the first time with a statistical significance of 7.6σ. Its branching fraction is measured to be $(2.64 \pm 0.32_{\rm stat} \pm 0.12_{\rm sys}) \times 10^{-6}$, where the first uncertainty is statistical and the second is systematic. The result is consistent with the previous measurement of its isospin partner process $\psi(3686) \to \Sigma^+\bar{\Sigma}^-\phi$, aligning with the naive expectation of isospin symmetry. In addition, we search for potential intermediate states in the $\Sigma^0\phi$ ($\bar{\Sigma}^0\phi$) invariant mass distribution and a possible threshold enhancement in the $\Sigma^0\bar{\Sigma}^0$ system, but no conclusive evidence of them is observed.

DOI: 10.1103/PhysRevD.111.052012

I. INTRODUCTION

Unlike the well-established theory of electromagnetic interactions, quantum chromodynamics (QCD) theory faces challenges in the nonperturbative region, where the theoretical calculations rely on approximations and models in various situations. As of today, there is still no universally accepted and reliable calculation technique of strong interactions in this region [1].

The charmonium states are usually interpreted as bound states consisting of a charm quark and an anticharm quark. Experimental studies of the hadronic decays of charmonium states, which lie between the perturbative and nonperturbative regimes, are important to test the current QCD theory and the theoretical models [2,3]. In the hadronic decays of charmonium states, especially the three-body decays, various intermediate states could be produced, and the properties of these states could be used to test the QCD-based theoretical framework.

The investigations of the decays of $\psi(3686) \to B\bar{B}P(V)$, where B denotes a baryon, $\bar{B}$ denotes its antiparticle and $P(V)$ denotes a pseudoscalar (vector) meson, are essential to search for intermediate states such as baryonium [4,5] and excited baryons that have not yet been observed [6,7].

In recent years, the decays $\psi(3686) \to \Lambda\bar{\Lambda}\pi^0$, $\Lambda\bar{\Lambda}\eta$ [8], $\Lambda\bar{\Lambda}\eta'$ [9], $\Lambda\bar{\Lambda}\omega$ [10], $\Sigma^+\bar{\Sigma}^-\omega$, $\Sigma^+\bar{\Sigma}^-\phi$ [11] and $\Sigma^+\bar{\Sigma}^-\eta$ [12] have been observed at BESIII. Evidence of the excited state Λ^* was found in $\psi(3686) \to \Lambda\bar{\Lambda}\omega$ with a significance of 3.0σ [10], and the excited state $\Lambda(1670)$ was observed with a significance larger than 5.0σ in the $\Lambda\eta$ system in $\psi(3686) \to \Lambda\bar{\Lambda}\eta$ [8]. Additionally, a near-threshold enhancement in the $\Lambda\bar{\Lambda}$ invariant mass spectrum was observed for the first time in $e^+e^- \to \Lambda\bar{\Lambda}\phi$ [13]. These exciting results stimulate us to search for such effects in the similar decay $\psi(3686) \to \Sigma^0\bar{\Sigma}^0\phi$.

In this paper, we report the first observation of the decay $\psi(3686) \to \Sigma^0\bar{\Sigma}^0\phi$ and measure its branching fraction using $(27.12 \pm 0.14) \times 10^8$ $\psi(3686)$ events [14]. In addition, we search for potential intermediate states in the $\Sigma^0\phi(\bar{\Sigma}^0\phi)$ invariant mass spectrum and a possible threshold enhancement in the $\Sigma^0\bar{\Sigma}^0$ system.

II. BESIII DETECTOR AND MONTE CARLO SIMULATION

The BESIII detector [15] records symmetric e^+e^- collisions provided by the BEPCII storage ring [16] in the center-of-mass energy range from 1.84 to 4.95 GeV, with a peak luminosity of 1.1×10^{33} cm^{-2} s^{-1} achieved at $\sqrt{s} = 3.773$ GeV. BESIII has collected large data samples in this energy region [17] [18]. The cylindrical core of the BESIII detector covers 93% of the full solid angle and consists of a helium-based multilayer drift chamber (MDC), a time-of-flight system (TOF), and a CsI (Tl) electromagnetic calorimeter (EMC), which are all enclosed in a superconducting solenoidal magnet providing a 1.0 T magnetic field. The magnet is supported by an octagonal flux-return yoke with modules of resistive plate muon counter interleaved with steel. The charged-particle momentum resolution at 1 GeV/c is 0.5%, and the specific ionization energy loss dE/dx resolution is 6% for the electrons from Bhabha scattering at 1 GeV. The EMC measures photon energy with a resolution of 2.5% (5%) at 1 GeV in the barrel (end cap) region. The time resolution of the TOF plastic scintillator barrel part is 68 ps, while that of

[*]Full author list given at the end of the article.

the end cap part was 110 ps. The end cap TOF system was upgraded in 2015 using multigap resistive plate chamber technology, providing a time resolution of 60 ps, which benefits ~83% of the data used in this analysis [19–21].

Monte Carlo (MC) simulated data samples produced with Geant4-based [22] software, which includes the geometric description [23] of the BESIII detector and the detector response, are used to optimize the event selection criteria, determine the detection efficiencies and study the background components. The simulation models the beam energy spread and initial-state radiation in the e^+e^- annihilations using the generator KKMC [24,25]. The inclusive MC sample includes the production of the $\psi(3686)$ resonance, the initial-state radiation production of the J/ψ, and the continuum processes incorporated in KKMC. All particle decays are modeled by EvtGen [26,27] using branching fractions either taken from the Particle Data Group (PDG) [28], when available, or otherwise estimated with LundCharm [29,30]. Final-state radiation from charged final-state particles is included using PHOTOS [31]. The signal MC sample, consisting of 3.0×10^6 events, is generated using a phase space model (PHSP) to determine the detection efficiency. The data sample collected at the center-of-mass energy of $\sqrt{s} = 3.650$ GeV, corresponding to an integrated luminosity of 401 pb^{-1} [14], is used to study the continuum background.

III. EVENT SELECTION AND BACKGROUND ANALYSIS

The decay modes $\Sigma^0 \to \gamma\Lambda$, $\Lambda \to p\pi^-$ ($\bar{\Sigma}^0 \to \gamma\bar{\Lambda}$, $\bar{\Lambda} \to \bar{p}\pi^+$) and $\phi \to K^+K^-$, which have large branching fractions and high reconstruction efficiency, are selected to reconstruct our signal process. To further increase the efficiency, we apply a partial reconstruction method, where either the $\bar{\Sigma}^0$ baryon or the Σ^0 baryon is not reconstructed but instead identified by the recoiling mass of the reconstructed particles. The tag method missing the $\bar{\Sigma}^0$ is referred to as "tag A," and the method missing the Σ^0 is referred to as "tag B." To avoid double counted events, tag B is used only when tag A is not feasible. For example, if the Λ baryon cannot be reconstructed due to a missing proton or π^- meson, reconstructing the Σ^0 is also not possible, and as a result, we turn to tag B. The events selected by tag A or tag B are analyzed separately.

Each candidate event is required to contain at least two positive and two negative charged tracks and at least one candidate photon. Additionally, the polar angle (θ) of the charged tracks detected by the MDC must be in the range $|\cos\theta| \leq 0.93$, where θ is defined with respect to the z axis, i.e., the symmetry axis of the MDC.

Photon candidates are identified using showers in the EMC. The deposited energy of each shower must be greater than 25 MeV in the barrel region ($|\cos\theta| < 0.80$) or greater than 50 MeV in the end cap region ($0.86 < |\cos\theta| < 0.92$). To suppress electronic noise and energy depositions not associated with the event, we further require the EMC cluster time from the reconstructed event start time to fall within the range [0, 700] ns. To veto showers originating from charged tracks, the opening angle between the extrapolated trajectory of any charged track and the shower position must exceed 10 degrees.

Particle identification for charged tracks combines measurements of $\mathrm{d}E/\mathrm{d}x$ in the MDC and the flight time in the TOF to calculate the probability $P(h)(h = p, K, \pi)$ for each particle type hypothesis. The track with the highest probability of being a proton is assumed to be a proton, i.e., $P(p) > P(K)$ and $P(p) > P(\pi)$, while pions are identified by requiring $P(\pi) > P(K)$ and $P(\pi) > P(p)$. The remaining tracks that are not identified as a proton or pion are assumed to be kaons originating from the ϕ meson. Each candidate signal event is required to contain exactly one K^+ and one K^-. Additionally, we require $N_{\pi^-} = 1$, $N_p = 1$, $N_{\pi^+} < 2$, and $N_{\bar{p}} < 2$ for candidate events in tag A, and $N_{\pi^+} = 1$, $N_{\bar{p}} = 1$, $N_{\pi^-} < 2$, and $N_p < 2$ for candidate events in tag B, where N denotes the number of different particles in the event. We limit the numbers of p and π of the recoiling side to suppress the background.

The charged tracks assumed to be kaons originating from the ϕ decay are required to satisfy $|V_z| < 10$ cm and $|V_{xy}| < 1$ cm, where $|V_z|$ is the distance of closest approach to the interaction point along the z direction and V_{xy} is the distance in the transverse x-y plane. A vertex fit is performed on the K^+K^- pair to reconstruct the ϕ meson. A secondary vertex fit is performed on the $p\pi^-(\bar{p}\pi^+)$ pair to reconstruct the $\Lambda(\bar{\Lambda})$ state. The $\Lambda(\bar{\Lambda})$ decay length, defined as the distance of the $\Lambda(\bar{\Lambda})$ decay vertex from the interaction point, is required to be greater than zero. Additionally, the χ^2 value of the secondary vertex fit is required to be less than 30. The surviving events are required to fall within $|M_{p\pi^-(\bar{p}\pi^+)} - m_{\Lambda(\bar{\Lambda})}| < 0.006$ GeV/c^2 (4 standard deviations), as shown in Fig. 1, where $M_{p\pi^-(\bar{p}\pi^+)}$ is the invariant mass of the $p\pi$ pair and $m_{\Lambda(\bar{\Lambda})}$ is the $\Lambda(\bar{\Lambda})$ mass [28].

In the signal channel, the Σ^0 and $\bar{\Sigma}^0$ states always appear in pairs and the proper photon should make the reconstructed mass of $\gamma\Lambda$ ($\gamma\bar{\Lambda}$) close to the recoil mass of $\gamma\Lambda\phi$ ($\gamma\bar{\Lambda}\phi$). For tag A, the candidate photon is selected by minimizing the variable $\Delta = (M_{\gamma\Lambda} - M^{\mathrm{rec}}_{\gamma\Lambda\phi})^2$, where $M_{\gamma\Lambda}$ is the invariant mass of $\gamma\Lambda$ and $M^{\mathrm{rec}}_{\gamma\Lambda\phi}$ is the recoiling mass of $\gamma\Lambda\phi$. The photon in tag B is selected similarly by minimizing $\Delta = (M_{\gamma\bar{\Lambda}} - M^{\mathrm{rec}}_{\gamma\bar{\Lambda}\phi})^2$.

The background components are studied with the $\psi(3686)$ inclusive MC sample using TopoAna [32]; the remaining events can be categorized into eight types depending on their distinctive peaking characteristics, as summarized in Table I. Here, "non-ϕ" indicates that the ϕ peak is not observed in the decay chain of the background,

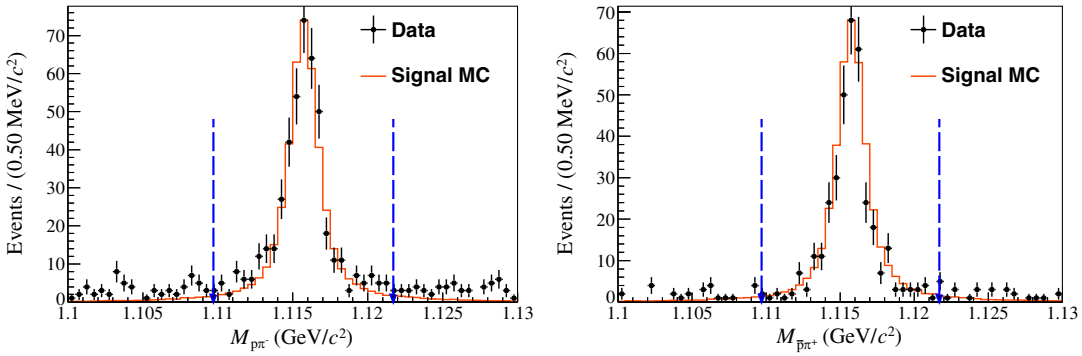

FIG. 1. Left: distribution of $M_{p\pi^-}$ for tag A. Right: distribution of $M_{\bar{p}\pi^+}$ for tag B. The dots with error bars are data, the orange solid lines represent the signal MC sample, and the blue dashed lines show the required range.

and "non-Σ^0" and "non-$\bar{\Sigma}^0$" have similar meanings. Type 6 and type 7 events are the dominant background sources, while the contributions from types 1–5 are relatively negligible. Specifically, the dominant background channels of type 6 events are the decays $\chi_{cJ}(J = 0, 1, 2) \to \Lambda\bar{\Lambda}\phi$, while for type 7 events they are the decays $\chi_{cJ} \to \bar{\Omega}^+\Omega^-$.

The yields of the continuum background events are estimated using the data sample collected at $\sqrt{s} = 3.650$ GeV. Only a few events survive and no peaking contribution is observed, indicating that the continuum background is negligible.

IV. BRANCHING FRACTION MEASUREMENT

For simplicity, the notations below are used interchangeably: $M_{K^+K^-}$ as M_ϕ, $M_{\gamma\Lambda}$ and $M^{\rm rec}_{\gamma\bar{\Lambda}\phi}$ as M^0_Σ, and $M_{\gamma\bar{\Lambda}}$ and $M^{\rm rec}_{\gamma\Lambda\phi}$ as $M^0_{\bar{\Sigma}}$. A topological analysis has shown the presence of non-negligible peaking background in the Σ^0, $\bar{\Sigma}^0$ and ϕ mass distributions concurrently. In addition, a correlation is observed between M_{Σ^0} and $M_{\bar{\Sigma}^0}$, due to the photon selection. Therefore, to determine the number of signal events, we perform an extended unbinned maximum likelihood three-dimensional fit on the M_ϕ and $M^{\rm 2D}_{\Sigma^0\bar{\Sigma}^0}$ distributions of the accepted candidate events in the data, where $M^{\rm 2D}_{\Sigma^0\bar{\Sigma}^0}$ represents the two-dimensional distribution of M_{Σ^0} versus $M_{\bar{\Sigma}^0}$. Table II lists the probability distribution function (PDF) models used in the fit. Here, type 0 events of Table I are divided into two components: one retains the name "type 0," denoting the signal corrected by MC truth matching technique, while the other, labeled as "mismatch," denotes the incorrect combination background of the signal decay. The type 2, type 3 and type 6 events are identical to those in Table I. The type 8 incorporates type 1, type 4 and type 5 events of Table I, denoting all the non-ϕ backgrounds. The M_ϕ and $M^{\rm 2D}_{\Sigma^0\bar{\Sigma}^0}$ signal shapes are derived from the signal MC sample with the RooKeysPdf and RooNDKeysPdf functions, which are one-dimensional and multidimensional Gaussian kernel density estimators [33] implemented in ROOT, respectively. The non-ϕ background shape is described by a reverse ARGUS [34] function, defined as

$$\mathrm{ARGUS}(m; m_0, \xi, p) = \begin{cases} 0 & (m < m_0), \\ m \cdot \nu^p \cdot e^{\xi\cdot\nu} & (m \geq m_0), \end{cases} \quad (1)$$

where m is the K^+K^- invariant mass, m_0 is the mass threshold, $\nu = (\frac{m}{m_0})^2 - 1$, and p and ξ are free parameters. For type 2, type 3 and type 6 events, the $M^{\rm 2D}_{\Sigma^0\bar{\Sigma}^0}$ distributions are derived from the inclusive MC sample with the RooNDKeysPdf function. For type 8 events, the $M^{\rm 2D}_{\Sigma^0\bar{\Sigma}^0}$

TABLE I. Numbers of surviving events in the $\psi(3686)$ inclusive MC sample after selections.

Event type				Tag A	Tag B
Type 0	ϕ	Σ^0	$\bar{\Sigma}^0$	452	430
Type 1	Non-ϕ	Σ^0	$\bar{\Sigma}^0$	1	1
Type 2	ϕ	Σ^0	Non-$\bar{\Sigma}^0$	44	40
Type 3	ϕ	Non-Σ^0	$\bar{\Sigma}^0$	46	46
Type 4	Non-ϕ	Σ^0	Non-$\bar{\Sigma}^0$	18	1
Type 5	Non-ϕ	Non-Σ^0	$\bar{\Sigma}^0$	4	10
Type 6	ϕ	Non-Σ^0	Non-$\bar{\Sigma}^0$	6090	4866
Type 7	Non-ϕ	Non-Σ^0	Non-$\bar{\Sigma}^0$	335	246

TABLE II. PDF models used in the three-dimensional fit. In the table, "signal MC" and "inclusive MC" correspond to PDF models derived from the MC simulation shapes, while "ϕ sideband" PDF is derived from the data.

Event type				M_ϕ	$M^{\rm 2D}_{\Sigma^0\bar{\Sigma}^0}$
Type 0	ϕ	Σ^0	$\bar{\Sigma}^0$	Signal MC	Signal MC
Mismatch	Wrong combinations			Signal MC	Signal MC
Type 2	ϕ	Σ^0	Non-$\bar{\Sigma}^0$	Signal MC	Inclusive MC
Type 3	ϕ	Non-Σ^0	$\bar{\Sigma}^0$	Signal MC	Inclusive MC
Type 6	ϕ	Non-Σ^0	Non-$\bar{\Sigma}^0$	Signal MC	Inclusive MC
Type 8	Non-ϕ			ARGUS	ϕ sideband

distribution is derived from the ϕ sideband events of the data sample with the RooNDKeysPdf function.

In the three-dimensional fit, the numbers of type 2 and type 3 events are fixed according to their fractions derived from the inclusive MC samples, and normalized to the data sample. Additionally, the ratio between the numbers of mismatched events and correct events is fixed to its value in the signal MC sample. The left-free parameters include the numbers of signal, type 6 and type 8 events, and three parameters of the ARGUS function. The fit results are shown in Figs. 2 and 3.

From this fit, the number of signal events is determined to be 57.3 ± 9.7 for tag A and 50.8 ± 9.1 for tag B. The statistical significances of tag A and tag B are estimated from the differences in the log-likelihood values with and without the signal function, and are 6.2σ and 6.3σ, respectively. The significance of the combined signal from tag A and tag B is 7.6σ.

The branching fraction of $\psi(3686) \to \Sigma^0\bar{\Sigma}^0\phi$ is calculated as

$$\mathcal{B}(\psi(3686) \to \Sigma^0\bar{\Sigma}^0\phi) = \frac{N_{\rm sig}^{\rm obs}}{N_{\psi(3686)} \cdot \varepsilon_{\rm sig} \cdot \mathcal{B}_\phi}, \quad (2)$$

where $N_{\rm sig}^{\rm obs}$ is the number of signal events, $\mathcal{B}_\phi$ is the branching fraction of $\phi \to K^+K^-$ [28], $\varepsilon_{\rm sig}$ is the signal efficiency determined by the MC simulation and the number of $\psi(3686)$ events in data is $N_{\psi(3686)} = (27.12 \pm 0.14) \times 10^8$ [35]. The branching fraction of $\Sigma^0 \to \gamma\Lambda$ is 100% according to the PDG, and thus it is not included in Eq. (2). The branching fractions of $\Lambda \to p\pi^-$ and $\bar{\Lambda} \to \bar{p}\pi^+$ are not in the formula either, as they have been incorporated into the signal efficiency. The weighted statistical uncertainty ($\sigma_{\rm stat}$) and the average value (μ) of tag A and tag B are calculated as

$$\frac{1}{\sigma_{\rm stat}^2} = \frac{1}{\sigma_A^2} + \frac{1}{\sigma_B^2} \quad \text{and} \quad \mu = \sigma_{\rm stat}^2\left(\frac{\mu_A}{\sigma_A^2} + \frac{\mu_B}{\sigma_B^2}\right), \quad (3)$$

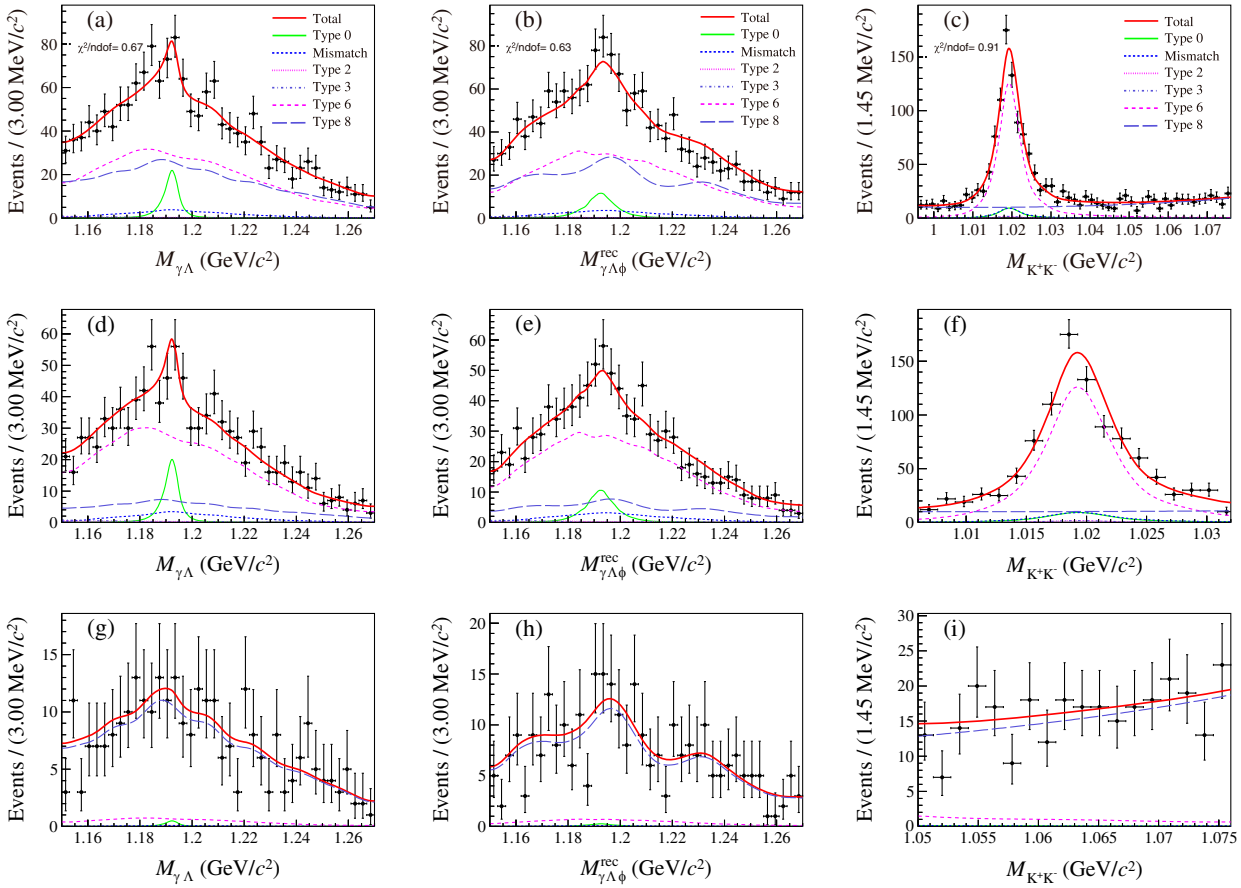

FIG. 2. Fit results and projections for tag A. Top: projections in the full range of $M_{K^+K^-}$: (a) $M_{\gamma\Lambda}$, (b) $M^{\rm rec}_{\gamma\Lambda\phi}$, and (c) $M_{K^+K^-}$. Middle: projections in the $M_{K^+K^-}$ signal region (1.006–1.032 GeV/c^2): (d)–(f). Bottom: projections in the $M_{K^+K^-}$ sideband region (1.050–1.076 GeV/c^2): (g)–(i). The dots with error bars (black), wide solid lines (red), narrow solid lines (green), dashed lines (blue), dotted lines (magenta), dash-dotted lines (bluish violet), extended dashed lines (magenta), and long-dashed lines (bluish violet) stand for the data, total fit, signal events, mismatched events, type 2 events, type 3 events, type 6 events, and type 8 events, respectively.

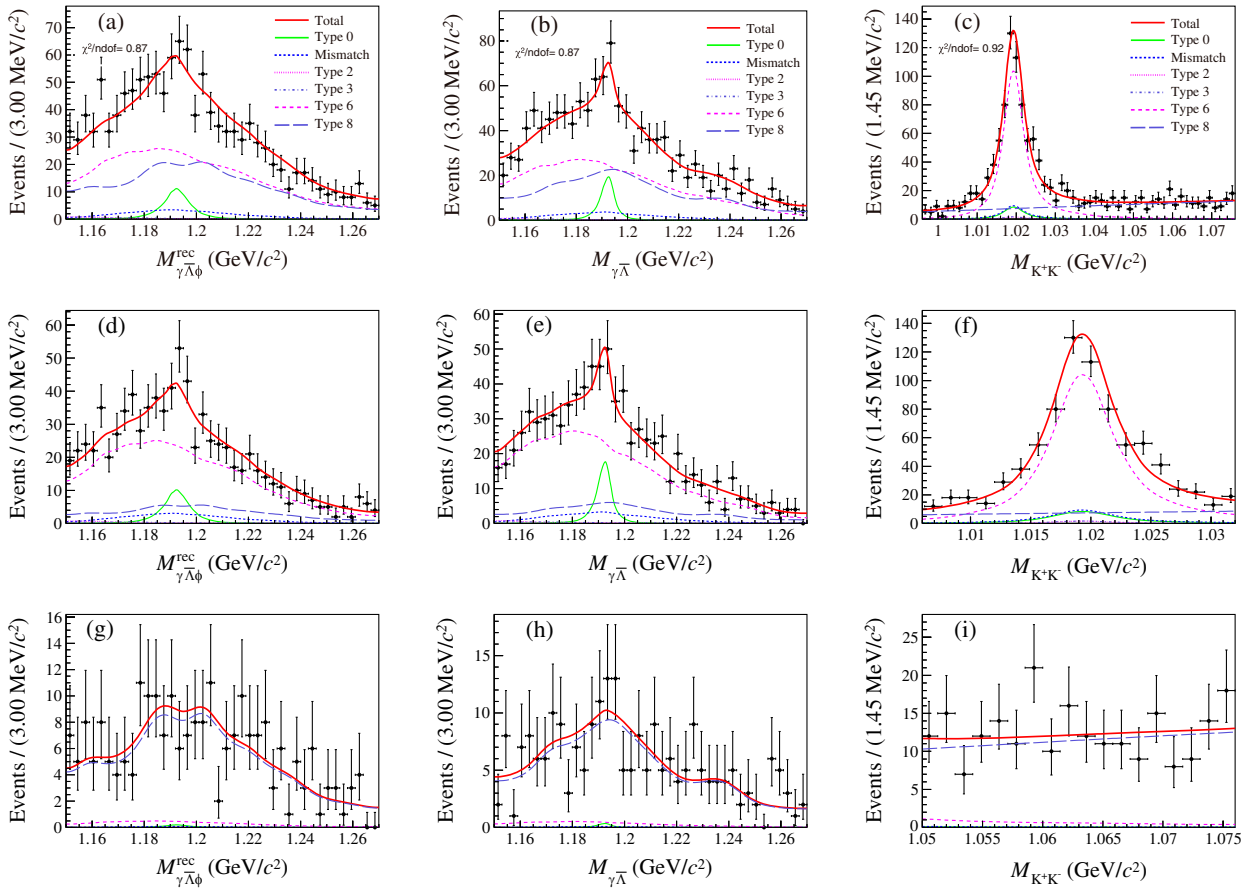

FIG. 3. Fit results and projections for tag B. Top: projections in the full range of $M_{K^+K^-}$: (a) $M^{\rm rec}_{\gamma\bar{\Lambda}\phi}$, (b) $M_{\gamma\bar{\Lambda}}$, and (c) $M_{K^+K^-}$. Middle: projections in the $M_{K^+K^-}$ signal region. Bottom: projections in the $M_{K^+K^-}$ sideband region.

where the subscripts "A" and "B" represent tag A and tag B accordingly. Table III lists the numerical results.

V. STUDY OF INTERMEDIATE STATES

In order to investigate potential intermediate states in $\psi(3686) \to \Sigma^0\bar{\Sigma}^0\phi$, candidate events of tag A and tag B are required to fall within the Σ^0, $\bar{\Sigma}^0$, and ϕ signal regions, as shown in Table IV. These signal regions are within 3 standard deviations around individual fitted masses. Tag A and Tag B are combined to increase the statistics. The distributions of $M_{\Sigma^0\phi}$, $M_{\bar{\Sigma}^0\phi}$ and $M_{\Sigma^0\bar{\Sigma}^0}$, as well as the Dalitz plots of $M^2_{(\Sigma^0\phi)}$ versus $M^2_{(\bar{\Sigma}^0\phi)}$, are shown in Fig. 4. In the $M_{\Sigma^0\bar{\Sigma}^0}$ spectrum, a difference between the PHSP MC and the data is observed around 2.43 GeV. However, due to the limited statistics, we are unable to draw a definitive conclusion. Additional data and further research are required.

TABLE III. Signal yield in the data, statistical significance, detection efficiency and branching fraction.

	Signal yield	Significance	ε (%)	$\mathcal{B}(\times 10^{-6})$
Tag A	57.3 ± 9.7	6.2σ	1.69	2.54 ± 0.43
Tag B	50.8 ± 9.1	6.3σ	1.38	2.76 ± 0.50
Average				2.63 ± 0.32

VI. SYSTEMATIC UNCERTAINTIES

The sources of systematic uncertainties on the measured branching fraction are described below.

(1) *Kaon tracking*

The uncertainty of kaon tracking is assigned as 1.0% per kaon from the study of the control sample $J/\psi \to K^0_S K^\pm \pi^\mp$ [36].

TABLE IV. Signal regions of tag A and tag B.

		Signal region (GeV/c^2)
Tag A	$M_{\gamma\Lambda}$	[1.176, 1.207]
	$M^{\rm rec}_{\gamma\Lambda\phi}$	[1.174, 1.210]
	$M_{K^+K^-}$	[1.006, 1.032]
Tag B	$M^{\rm rec}_{\gamma\bar{\Lambda}\phi}$	[1.175, 1.209]
	$M_{\gamma\bar{\Lambda}}$	[1.177, 1.207]
	$M_{K^+K^-}$	[1.006, 1.032]

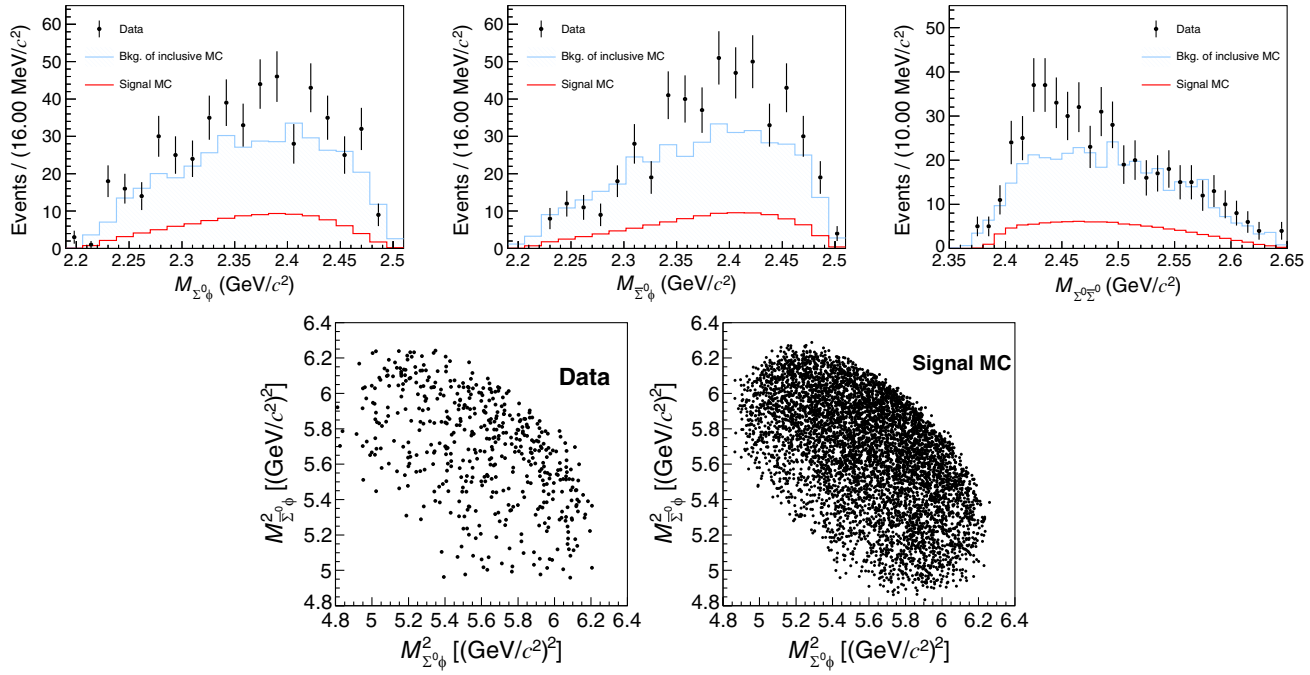

FIG. 4. Top: distributions of $M_{\Sigma^0\phi}$, $M_{\bar{\Sigma}^0\phi}$ and $M_{\Sigma^0\bar{\Sigma}^0}$ in the data and MC samples. The black dots with error bars are data, the red curves denote the PHSP MC simulated shape and the shadowed blue areas denote the backgrounds obtained from the inclusive MC sample. The signal and background are normalized according to the numbers of events in the data. Bottom: Dalitz plots of $M^2_{\Sigma^0\phi}$ versus $M^2_{\bar{\Sigma}^0\phi}$ in the data and signal MC samples.

(2) *Photon detection*

The uncertainty of photon reconstruction is assigned as 0.5% per photon based on the study of the control sample $e^+e^- \to \gamma\mu^+\mu^-$ [37].

(3) $\Lambda(\bar{\Lambda})$ *reconstruction*

The uncertainty of $\Lambda(\bar{\Lambda})$ reconstruction includes the uncertainty of tracking and particle identification for p and π, along with the decay length and the χ^2 value requirements. The efficiency of $\Lambda(\bar{\Lambda})$ reconstruction depends on its polar angle and momentum distributions, and the distributions of the signal MC sample differ slightly from those of the data sample. We use the control sample $J/\psi \to pK^-\bar{\Lambda} + \text{c.c.}$ [38] to correct the efficiency and estimate the uncertainty, which is determined to be 1.0% (0.8%) for tag A (B).

(4) $\Lambda(\bar{\Lambda})$ *mass window*

We fit the data sample using the simulated shape convolved with a Gaussian resolution function. After smearing this Gaussian resolution function to the signal MC sample, the change in the efficiency is estimated as the related uncertainty, and it is 0.2% (0.2%) for tag A (B).

(5) *Wrong combination ratio*

The wrong combination ratio of the signal MC sample may vary from that of the data sample. We adjust the matching angle in the MC truth association by $\pm 1°$ [39] and take the larger change of the re-measured branching fractions as the systematic uncertainty, which is 0.8% (1.4%) for tag A (B).

(6) *MC sample size*

The relative uncertainty of the signal MC sample size is estimated as $\sqrt{\frac{1-\varepsilon}{N\cdot\varepsilon}}$, where ε is the detection efficiency and N is the total number of the generated signal events. It is 0.4% (0.5%) for tag A (B).

(7) *Fit procedure*

(a) *Fit range*: We simultaneously vary the fit range of M_{Σ^0}, $M_{\bar{\Sigma}^0}$ and M_ϕ by ± 10 MeV/c^2, except for the lower limit of M_ϕ, as there is a threshold. The larger difference in the remeasured branching fraction is assigned as the uncertainty, which is 4.5% (2.6%) for tag A (B).

(b) *Fixed numbers of background events*: Assuming that the number of type 2 events follows a Poisson distribution, we adjust it by $\pm\sqrt{N_2}$, where N_2 denotes the number of type 2 events that is fixed in the fit. Alternative fits are performed with modified N_2 and the larger difference in the branching fraction is assigned as the uncertainty. It is 0.6% (0.4%) for tag A (B). The uncertainty associated with the number of type 3 events is estimated similarly, which is 0.6% (0.2%) for tag A (B).

(c) *Signal shape*: The description of the ϕ shape is changed from the RooKeysPdf function to the RooHistPdf function. At the same time, the

overall scale factor of the bandwidth of the RooNDKeysPdf function is varied from 1.0 to 1.3, representing the uncertainty of the $M^{2D}_{\Sigma^0\bar{\Sigma}^0}$ shape. The uncertainty associated with the signal shape is assigned as 1.7% (0.6%) for tag A (B).

(d) *Background shape*: The uncertainties of the shapes of the type 2 and type 3 events are negligible. For the shape of type 8 events, the smooth shape of $M_{K^+K^-}$ is replaced by a second-order Chebyshev polynomial function, and the $M^{2D}_{\Sigma^0\bar{\Sigma}^0}$ distribution is changed by moving the ϕ sideband range by $10\ \mathrm{MeV}/c^2$ towards the higher mass region. As for the shapes of the type 6 and mismatched events, their ϕ shapes are changed to the RooHistPdf function instead of the RooKeysPdf function, and the distributions of $M^{2D}_{\Sigma^0\bar{\Sigma}^0}$ are varied by changing the bandwidth scale factor of the RooNDKeysPdf function from 1.0 to 1.3. The difference in the branching fraction after modifying the background shape is considered as the uncertainty, and it is 1.4% (3.5%) for tag A (B).

(8) *Quoted branching fractions*

The uncertainties of $\mathcal{B}(\Lambda \to p\pi^-/\bar{\Lambda} \to \bar{p}\pi^+)$ and $\mathcal{B}(\phi \to K^+K^-)$ are taken from the PDG [28], which are 0.8% and 1.0%, respectively.

(9) *Number of $\psi(3686)$ events*

The uncertainty of the total number of $\psi(3686)$ events in the data sample is 0.5% [14,35].

The correlations of the uncertainties between tag A and tag B are considered. We divide the uncertainties into uncorrelated individual uncertainties and correlated common uncertainties, which include kaon tracking, photon detection, quoted branching fractions, number of $\psi(3686)$ events, and $\Lambda(\bar{\Lambda})$ reconstruction. For a conservative estimation, we assume full correlation for the correlated uncertainties. All the systematic uncertainty sources and their values are summarized in Table V.

Taking tag A and tag B as two independent measurements, the covariance matrix (V) of $\mathcal{B}_A$ and $\mathcal{B}_B$ is

$$V = \begin{bmatrix} (\sigma^A_{\mathrm{sys}} \cdot \mathcal{B}_A)^2 + {\sigma^A_{\mathrm{stat}}}^2 & (\sigma^A_{\mathrm{sys,c}} \cdot \mathcal{B}_A)(\sigma^B_{\mathrm{sys,c}} \cdot \mathcal{B}_B) \\ (\sigma^A_{\mathrm{sys,c}} \cdot \mathcal{B}_A)(\sigma^B_{\mathrm{sys,c}} \cdot \mathcal{B}_B) & (\sigma^B_{\mathrm{sys}} \cdot \mathcal{B}_B)^2 + {\sigma^B_{\mathrm{stat}}}^2 \end{bmatrix}, \tag{4}$$

in which $\mathcal{B}$ denotes the branching fraction of one single tag, $\sigma_{\mathrm{sys,c}}$ denotes the correlated systematic uncertainty, σ_{sys} denotes the sum of correlated and uncorrelated systematic uncertainties, and σ_{stat} denotes the statistical uncertainty. The scripts "A" and "B" represent tag A and tag B, respectively. Giving the covariance matrix, the least square method is applied to calculate the weighted average and the uncertainty of the branching fraction, as

TABLE V. Systematic uncertainties of the branching fraction measurement.

Source	Tag A (%)	Tag B (%)
Kaon tracking	2.0	2.0
Photon detection	0.5	0.5
Λ reconstruction	1.0	...
$\bar{\Lambda}$ reconstruction	...	0.8
Λ mass window	0.2	...
$\bar{\Lambda}$ mass window	...	0.2
Wrong combination ratio	0.8	1.4
MC sample size	0.4	0.5
Fit range	4.5	2.6
Number of type 2 events	0.6	0.4
Number of type 3 events	0.6	0.2
Signal shape	1.7	0.6
Background shape	1.4	3.5
Quoted ϕ branching fraction	1.0	1.0
Quoted Λ ($\bar{\Lambda}$) branching fraction	0.8	0.8
Number of $\psi(3686)$ events	0.5	0.5
Individual uncertainty	5.2	4.7
Common uncertainty	2.7	2.6
Total	5.9	5.4

$$\begin{aligned}\hat{\mathcal{B}} &= \left[\sum_{i,j=1}^{2}(V^{-1})_{ij}\right]^{-1}\left[\sum_{i,j=1}^{2}(V^{-1})_{ij}\mathcal{B}_j\right] \\ &= \frac{(V^{-1})_{11}\mathcal{B}_A + (V^{-1})_{12}\mathcal{B}_B + (V^{-1})_{21}\mathcal{B}_A + (V^{-1})_{22}\mathcal{B}_B}{(V^{-1})_{11} + (V^{-1})_{12} + (V^{-1})_{21} + (V^{-1})_{22}} \\ &\approx 2.64 \times 10^{-6}\end{aligned} \tag{5}$$

and

$$\begin{aligned}\hat{\sigma}^2_{\mathcal{B}} &= \left[\sum_{i,j=1}^{2}(V^{-1})_{ij}\right]^{-1} \\ &= ((V^{-1})_{11} + (V^{-1})_{12} + (V^{-1})_{21} + (V^{-1})_{22})^{-1}, \\ \hat{\sigma}_{\mathcal{B},\mathrm{sys}} &= \sqrt{\hat{\sigma}_{\mathcal{B}}{}^2 - {\sigma_{\mathcal{B},\mathrm{stat}}}^2} \\ &\approx 0.12 \times 10^{-6},\end{aligned} \tag{6}$$

where $\hat{\mathcal{B}}$ represents the expected value of the branching fraction, $\hat{\sigma}_{\mathcal{B}}$ represents the total uncertainty, $\sigma_{\mathcal{B},\mathrm{stat}}$ represents the statistical uncertainty in Table III and $\hat{\sigma}_{\mathcal{B},\mathrm{sys}}$ represents the overall systematic uncertainty.

VII. SUMMARY

Using $(27.12 \pm 0.14) \times 10^8$ $\psi(3686)$ events collected with the BESIII detector in 2009, 2012 and 2021, the decay $\psi(3686) \to \Sigma^0\bar{\Sigma}^0\phi$ is observed for the first time with a significance of 7.6σ. The branching fraction of this decay is measured to be $(2.64 \pm 0.32_{\mathrm{stat}} \pm 0.12_{\mathrm{sys}}) \times 10^{-6}$. The measured branching fraction is consistent with the previous

measurement of the isospin partner process $\psi(3686) \to \Sigma^+\bar{\Sigma}^-\phi$ [11]. The principle of isospin conservation is upheld within 1 standard deviation. Possible structures in the $\Sigma^0\bar{\Sigma}^0$ and $\Sigma^0\phi(\bar{\Sigma}^0\phi)$ invariant mass spectra have been investigated. However, with the current statistics, no conclusive evidence is observed.

ACKNOWLEDGMENTS

The BESIII Collaboration thanks the staff of BEPCII and the IHEP computing center for their strong support. This work is supported in part by National Key R&D Program of China under Contracts No. 2020YFA0406300, No. 2020YFA0406400, No. 2023YFA1606000; National Natural Science Foundation of China (NSFC) under Contracts No. 11635010, No. 11735014, No. 11935015, No. 11935016, No. 11935018, No. 12025502, No. 12035009, No. 12035013, No. 12061131003, No. 12192260, No. 12192261, No. 12192262, No. 12192263, No. 12192264, No. 12192265, No. 12221005, No. 12225509, No. 12235017, No. 12361141819; the Chinese Academy of Sciences (CAS) Large-Scale Scientific Facility Program; the CAS Center for Excellence in Particle Physics (CCEPP); Joint Large-Scale Scientific Facility Funds of the NSFC and CAS under Contract No. U1832207; 100 Talents Program of CAS; The Institute of Nuclear and Particle Physics (INPAC) and Shanghai Key Laboratory for Particle Physics and Cosmology; German Research Foundation DFG under Contracts Nos. 455635585, FOR5327, GRK 2149; Istituto Nazionale di Fisica Nucleare, Italy; Ministry of Development of Turkey under Contract No. DPT2006K-120470; National Research Foundation of Korea under Contract No. NRF-2022R1A2C1092335; National Science and Technology fund of Mongolia; National Science Research and Innovation Fund (NSRF) via the Program Management Unit for Human Resources & Institutional Development, Research and Innovation of Thailand under Contract No. B16F640076; Polish National Science Centre under Contract No. 2019/35/O/ST2/02907; The Swedish Research Council; U.S. Department of Energy under Contract No. DE-FG02-05ER41374.

DATA AVAILABILITY

The data that support the findings of this article are not publicly available. The data are available from the authors upon reasonable request.

[1] S. Narison, *QCD as a Theory of Hadrons: From Partons to Confinement* (Cambridge University Press, New York, 2004).
[2] V. A. Novikov, L. B. Okun, M. A. Shifman, A. I. Vainshtein, M. B. Voloshin, and V. I. Zakharov, Phys. Rep. **41** (1978).
[3] N. Brambilla *et al.*, Eur. Phys. J. C **71**, 1534 (2011).
[4] C. Hong-Mo and H. Hogaasen, Nucl. Phys. **B136**, 401 (1978).
[5] W. Bing-Song, Z. Sheng-Qi, and Q. Cong-Feng, Phys. Rev. D **105**, 014016 (2022).
[6] A. V. Sarantsev, M. Matveev, V. A. Nikonov, A. V. Anisovich, U. Thoma, and E. Klempt, Eur. Phys. J. A **55**, 180 (2019).
[7] V. Crede, AIP Conf. Proc. **2249**, 020003 (2020).
[8] M. Ablikim *et al.* (BESIII Collaboration), Phys. Rev. D **106**, 072006 (2022).
[9] M. Ablikim *et al.* (BESIII Collaboration), Phys. Rev. D **108**, 112014 (2023).
[10] M. Ablikim *et al.* (BESIII Collaboration), Phys. Rev. D **106**, 112011 (2022).
[11] M. Ablikim *et al.* (BESIII Collaboration), Phys. Rev. D **108**, 092011 (2023).
[12] M. Ablikim *et al.* (BESIII Collaboration), Phys. Rev. D **106**, 112007 (2022).
[13] M. Ablikim *et al.* (BESIII Collaboration), Phys. Rev. D **104**, 052006 (2021).
[14] M. Ablikim *et al.* (BESIII Collaboration), Chin. Phys. C **48**, 093001 (2024).
[15] M. Ablikim *et al.* (BESIII Collaboration), Nucl. Instrum. Methods Phys. Res., Sect. A **614**, 345 (2010).
[16] C. H. Yu *et al.*, *Proceedings of IPAC2016, Busan, Korea* (2016), 10.18429/JACoW-IPAC2016-TUYA01.
[17] M. Ablikim *et al.* (BESIII Collaboration), Chin. Phys. C **44**, 040001 (2020).
[18] J. W. Zhang, L. H. Wu, S. S. Sun *et al.*, Radiat. Detect. Technol. Methods **6**, 289 (2022).
[19] X. Li *et al.*, Radiat. Detect. Technol. Methods **1**, 13 (2017).
[20] Y. X. Guo *et al.*, Radiat. Detect. Technol. Methods **1**, 15 (2017).
[21] P. Cao *et al.*, Nucl. Instrum. Methods Phys. Res., Sect. A **953**, 163053 (2020).
[22] S. Agostinelli *et al.* (GEANT4 Collaboration), Nucl. Instrum. Methods Phys. Res., Sect. A **506**, 250 (2003).
[23] K. X. Huang *et al.*, Nucl. Sci. Tech. **33**, 142 (2022).
[24] S. Jadach, B. F. L. Ward, and Z. Was, Comput. Phys. Commun. **130**, 260 (2000).
[25] S. Jadach, B. F. L. Ward, and Z. Was, Phys. Rev. D **63**, 113009 (2001).
[26] R. G. Ping, Chin. Phys. C **32**, 599 (2008).
[27] D. J. Lange, Nucl. Instrum. Methods Phys. Res., Sect. A **462**, 152 (2001).
[28] P. L. Workman *et al.* (Particle Data Group), Prog. Theor. Exp. Phys. **2022**, 083C01 (2022).

[29] J. C. Chen, G. S. Huang, X. R. Qi, D. H. Zhang, and Y. S. Zhu, Phys. Rev. D **62**, 034003 (2000).
[30] R. L. Yang, R. G. Ping, and H. Chen, Chin. Phys. Lett. **31**, 061301 (2014).
[31] E. Richter-Was, Phys. Lett. B **303**, 163 (1993).
[32] X. Y. Zhou, S. X. Du, G. Li, and C. P. Shen, Comput. Phys. Commun. **258**, 107540 (2021).
[33] K. S. Cranmer, Comput. Phys. Commun. **136**, 3 (2001).
[34] H. Albrecht *et al.* (ARGUS Collaboration), Phys. Lett. B **241**, 278 (1990).
[35] M. Ablikim *et al.* (BESIII Collaboration), Chin. Phys. C **42**, 023001 (2018).
[36] M. Ablikim *et al.* (BESIII Collaboration), Phys. Rev. D **83**, 112005 (2011).
[37] M. Ablikim *et al.* (BESIII Collaboration), Phys. Rev. D **109**, 032006 (2024).
[38] M. Ablikim *et al.* (BESIII Collaboration), Phys. Rev. D **108**, 112012 (2023).
[39] M. Ablikim *et al.* (BESIII Collaboration), Phys. Rev. D **100**, 051101 (2019).

M. Ablikim,[1] M. N. Achasov,[4,c] P. Adlarson,[76] O. Afedulidis,[3] X. C. Ai,[81] R. Aliberti,[35] A. Amoroso,[75a,75c] Q. An,[72,58,a] Y. Bai,[57] O. Bakina,[36] I. Balossino,[29a] Y. Ban,[46,h] H.-R. Bao,[64] V. Batozskaya,[1,44] K. Begzsuren,[32] N. Berger,[35] M. Berlowski,[44] M. Bertani,[28a] D. Bettoni,[29a] F. Bianchi,[75a,75c] E. Bianco,[75a,75c] A. Bortone,[75a,75c] I. Boyko,[36] R. A. Briere,[5] A. Brueggemann,[69] H. Cai,[77] X. Cai,[1,58] A. Calcaterra,[28a] G. F. Cao,[1,64] N. Cao,[1,64] S. A. Cetin,[62a] X. Y. Chai,[46,h] J. F. Chang,[1,58] G. R. Che,[43] G. Chelkov,[36,b] C. Chen,[43] C. H. Chen,[9] Chao Chen,[55] G. Chen,[1] H. S. Chen,[1,64] H. Y. Chen,[20] M. L. Chen,[1,58,64] S. J. Chen,[42] S. L. Chen,[45] S. M. Chen,[61] T. Chen,[1,64] X. R. Chen,[31,64] X. T. Chen,[1,64] Y. B. Chen,[1,58] Y. Q. Chen,[34] Z. J. Chen,[25,i] Z. Y. Chen,[1,64] S. K. Choi,[10] G. Cibinetto,[29a] F. Cossio,[75c] J. J. Cui,[50] H. L. Dai,[1,58] J. P. Dai,[79] A. Dbeyssi,[18] R. E. de Boer,[3] D. Dedovich,[36] C. Q. Deng,[73] Z. Y. Deng,[1] A. Denig,[35] I. Denysenko,[36] M. Destefanis,[75a,75c] F. De Mori,[75a,75c] B. Ding,[67,1] X. X. Ding,[46,h] Y. Ding,[34] Y. Ding,[40] J. Dong,[1,58] L. Y. Dong,[1,64] M. Y. Dong,[1,58,64] X. Dong,[77] M. C. Du,[1] S. X. Du,[81] Y. Y. Duan,[55] Z. H. Duan,[42] P. Egorov,[36,b] Y. H. Fan,[45] J. Fang,[59] J. Fang,[1,58] S. S. Fang,[1,64] W. X. Fang,[1] Y. Fang,[1] Y. Q. Fang,[1,58] R. Farinelli,[29a] L. Fava,[75b,75c] F. Feldbauer,[3] G. Felici,[28a] C. Q. Feng,[72,58] J. H. Feng,[59] Y. T. Feng,[72,58] M. Fritsch,[3] C. D. Fu,[1] J. L. Fu,[64] Y. W. Fu,[1,64] H. Gao,[64] X. B. Gao,[41] Y. N. Gao,[46,h] Yang Gao,[72,58] S. Garbolino,[75c] I. Garzia,[29a,29b] L. Ge,[81] P. T. Ge,[19] Z. W. Ge,[42] C. Geng,[59] E. M. Gersabeck,[68] A. Gilman,[70] K. Goetzen,[13] L. Gong,[40] W. X. Gong,[1,58] W. Gradl,[35] S. Gramigna,[29a,29b] M. Greco,[75a,75c] M. H. Gu,[1,58] Y. T. Gu,[15] C. Y. Guan,[1,64] A. Q. Guo,[31,64] L. B. Guo,[41] M. J. Guo,[50] R. P. Guo,[49] Y. P. Guo,[12,g] A. Guskov,[36,b] J. Gutierrez,[27] K. L. Han,[64] T. T. Han,[1] F. Hanisch,[3] X. Q. Hao,[19] F. A. Harris,[66] K. K. He,[55] K. L. He,[1,64] F. H. Heinsius,[3] C. H. Heinz,[35] Y. K. Heng,[1,58,64] C. Herold,[60] T. Holtmann,[3] P. C. Hong,[34] G. Y. Hou,[1,64] X. T. Hou,[1,64] Y. R. Hou,[64] Z. L. Hou,[1] B. Y. Hu,[59] H. M. Hu,[1,64] J. F. Hu,[56,j] S. L. Hu,[12,g] T. Hu,[1,58,64] Y. Hu,[1] G. S. Huang,[72,58] K. X. Huang,[59] L. Q. Huang,[31,64] X. T. Huang,[50] Y. P. Huang,[1] Y. S. Huang,[59] T. Hussain,[74] F. Hölzken,[3] N. Hüsken,[35] N. in der Wiesche,[69] J. Jackson,[27] S. Janchiv,[32] J. H. Jeong,[10] Q. Ji,[1] Q. P. Ji,[19] W. Ji,[1,64] X. B. Ji,[1,64] X. L. Ji,[1,58] Y. Y. Ji,[50] X. Q. Jia,[50] Z. K. Jia,[72,58] D. Jiang,[1,64] H. B. Jiang,[77] P. C. Jiang,[46,h] S. S. Jiang,[39] T. J. Jiang,[16] X. S. Jiang,[1,58,64] Y. Jiang,[64] J. B. Jiao,[50] J. K. Jiao,[34] Z. Jiao,[23] S. Jin,[42] Y. Jin,[67] M. Q. Jing,[1,64] X. M. Jing,[64] T. Johansson,[76] S. Kabana,[33] N. Kalantar-Nayestanaki,[65] X. L. Kang,[9] X. S. Kang,[40] M. Kavatsyuk,[65] B. C. Ke,[81] V. Khachatryan,[27] A. Khoukaz,[69] R. Kiuchi,[1] O. B. Kolcu,[62a] B. Kopf,[3] M. Kuessner,[3] X. Kui,[1,64] N. Kumar,[26] A. Kupsc,[44,76] W. Kühn,[37] J. J. Lane,[68] L. Lavezzi,[75a,75c] T. T. Lei,[72,58] Z. H. Lei,[72,58] M. Lellmann,[35] T. Lenz,[35] C. Li,[47] C. Li,[43] C. H. Li,[39] Cheng Li,[72,58] D. M. Li,[81] F. Li,[1,58] G. Li,[1] H. B. Li,[1,64] H. J. Li,[19] H. N. Li,[56,j] Hui Li,[43] J. R. Li,[61] J. S. Li,[59] K. Li,[1] K. L. Li,[19] L. J. Li,[1,64] L. K. Li,[1] Lei Li,[48] M. H. Li,[43] P. R. Li,[38,k,l] Q. M. Li,[1,64] Q. X. Li,[50] R. Li,[17,31] S. X. Li,[12] T. Li,[50] W. D. Li,[1,64] W. G. Li,[1,a] X. Li,[1,64] X. H. Li,[72,58] X. L. Li,[50] X. Y. Li,[1,64] X. Z. Li,[59] Y. G. Li,[46,h] Z. J. Li,[59] Z. Y. Li,[79] C. Liang,[42] H. Liang,[1,64] H. Liang,[72,58] Y. F. Liang,[54] Y. T. Liang,[31,64] G. R. Liao,[14] Y. P. Liao,[1,64] J. Libby,[26] A. Limphirat,[60] C. C. Lin,[55] D. X. Lin,[31,64] T. Lin,[1] B. J. Liu,[1] B. X. Liu,[77] C. Liu,[34] C. X. Liu,[1] F. Liu,[1] F. H. Liu,[53] Feng Liu,[6] G. M. Liu,[56,j] H. Liu,[38,k,l] H. B. Liu,[15] H. H. Liu,[1] H. M. Liu,[1,64] Huihui Liu,[21] J. B. Liu,[72,58] J. Y. Liu,[1,64] K. Liu,[38,k,l] K. Y. Liu,[40] Ke Liu,[22] L. Liu,[72,58] L. C. Liu,[43] Lu Liu,[43] M. H. Liu,[12,g] P. L. Liu,[1] Q. Liu,[64] S. B. Liu,[72,58] T. Liu,[12,g] W. K. Liu,[43] W. M. Liu,[72,58] X. Liu,[38,k,l] X. Liu,[39] Y. Liu,[81] Y. Liu,[38,k,l] Y. B. Liu,[43] Z. A. Liu,[1,58,64] Z. D. Liu,[9] Z. Q. Liu,[50] X. C. Lou,[1,58,64] F. X. Lu,[59] H. J. Lu,[23] J. G. Lu,[1,58] X. L. Lu,[1] Y. Lu,[7] Y. P. Lu,[1,58] Z. H. Lu,[1,64] C. L. Luo,[41] J. R. Luo,[59] M. X. Luo,[80] T. Luo,[12,g] X. L. Luo,[1,58] X. R. Lyu,[64] Y. F. Lyu,[43] F. C. Ma,[40] H. Ma,[79] H. L. Ma,[1] J. L. Ma,[1,64] L. L. Ma,[50] L. R. Ma,[67] M. M. Ma,[1,64] Q. M. Ma,[1] R. Q. Ma,[1,64] T. Ma,[72,58] X. T. Ma,[1,64] X. Y. Ma,[1,58] Y. M. Ma,[31] F. E. Maas,[18] I. MacKay,[70] M. Maggiora,[75a,75c] S. Malde,[70] Y. J. Mao,[46,h] Z. P. Mao,[1] S. Marcello,[75a,75c] Z. X. Meng,[67] J. G. Messchendorp,[13,65] G. Mezzadri,[29a] H. Miao,[1,64] T. J. Min,[42] R. E. Mitchell,[27] X. H. Mo,[1,58,64] B. Moses,[27] N. Yu. Muchnoi,[4,c] J. Muskalla,[35] Y. Nefedov,[36] F. Nerling,[18,e] L. S. Nie,[20] I. B. Nikolaev,[4,c] Z. Ning,[1,58] S. Nisar,[11,m]

Q. L. Niu,[38,k,l] W. D. Niu,[55] Y. Niu,[50] S. L. Olsen,[64] S. L. Olsen,[10,64] Q. Ouyang,[1,58,64] S. Pacetti,[28b,28c] X. Pan,[55] Y. Pan,[57] A. Pathak,[34] Y. P. Pei,[72,58] M. Pelizaeus,[3] H. P. Peng,[72,58] Y. Y. Peng,[38,k,l] K. Peters,[13,e] J. L. Ping,[41] R. G. Ping,[1,64] S. Plura,[35] V. Prasad,[33] F. Z. Qi,[1] H. Qi,[72,58] H. R. Qi,[61] M. Qi,[42] T. Y. Qi,[12,g] S. Qian,[1,58] W. B. Qian,[64] C. F. Qiao,[64] X. K. Qiao,[81] J. J. Qin,[73] L. Q. Qin,[14] L. Y. Qin,[72,58] X. P. Qin,[12,g] X. S. Qin,[50] Z. H. Qin,[1,58] J. F. Qiu,[1] Z. H. Qu,[73] C. F. Redmer,[35] K. J. Ren,[39] A. Rivetti,[75c] M. Rolo,[75c] G. Rong,[1,64] Ch. Rosner,[18] S. N. Ruan,[43] N. Salone,[44] A. Sarantsev,[36,d] Y. Schelhaas,[35] K. Schoenning,[76] M. Scodeggio,[29a] K. Y. Shan,[12,g] W. Shan,[24] X. Y. Shan,[72,58] Z. J. Shang,[38,k,l] J. F. Shangguan,[16] L. G. Shao,[1,64] M. Shao,[72,58] C. P. Shen,[12,g] H. F. Shen,[1,8] W. H. Shen,[64] X. Y. Shen,[1,64] B. A. Shi,[64] H. Shi,[72,58] H. C. Shi,[72,58] J. L. Shi,[12,g] J. Y. Shi,[1] Q. Q. Shi,[55] S. Y. Shi,[73] X. Shi,[1,58] J. J. Song,[19] T. Z. Song,[59] W. M. Song,[34,1] Y. J. Song,[12,g] Y. X. Song,[46,h,n] S. Sosio,[75a,75c] S. Spataro,[75a,75c] F. Stieler,[35] S. S. Su,[40] Y. J. Su,[64] G. B. Sun,[77] G. X. Sun,[1] H. Sun,[64] H. K. Sun,[1] J. F. Sun,[19] K. Sun,[61] L. Sun,[77] S. S. Sun,[1,64] T. Sun,[51,f] W. Y. Sun,[34] Y. Sun,[9] Y. J. Sun,[72,58] Y. Z. Sun,[1] Z. Q. Sun,[1,64] Z. T. Sun,[50] C. J. Tang,[54] G. Y. Tang,[1] J. Tang,[59] M. Tang,[72,58] Y. A. Tang,[77] L. Y. Tao,[73] Q. T. Tao,[25,i] M. Tat,[70] J. X. Teng,[72,58] V. Thoren,[76] W. H. Tian,[59] Y. Tian,[31,64] Z. F. Tian,[77] I. Uman,[62b] Y. Wan,[55] S. J. Wang,[50] B. Wang,[1] B. L. Wang,[64] Bo Wang,[72,58] D. Y. Wang,[46,h] F. Wang,[73] H. J. Wang,[38,k,l] J. J. Wang,[77] J. P. Wang,[50] K. Wang,[1,58] L. L. Wang,[1] M. Wang,[50] N. Y. Wang,[64] S. Wang,[38,k,l] S. Wang,[12,g] T. Wang,[12,g] T. J. Wang,[43] W. Wang,[73] W. Wang,[59] W. P. Wang,[35,58,72,o] X. Wang,[46,h] X. F. Wang,[38,k,l] X. J. Wang,[39] X. L. Wang,[12,g] X. N. Wang,[1] Y. Wang,[61] Y. D. Wang,[45] Y. F. Wang,[1,58,64] Y. L. Wang,[19] Y. N. Wang,[45] Y. Q. Wang,[1] Yaqian Wang,[17] Yi Wang,[61] Z. Wang,[1,58] Z. L. Wang,[73] Z. Y. Wang,[1,64] Ziyi Wang,[64] D. H. Wei,[14] F. Weidner,[69] S. P. Wen,[1] Y. R. Wen,[39] U. Wiedner,[3] G. Wilkinson,[70] M. Wolke,[76] L. Wollenberg,[3] C. Wu,[39] J. F. Wu,[1,8] L. H. Wu,[1] L. J. Wu,[1,64] X. Wu,[12,g] X. H. Wu,[34] Y. Wu,[72,58] Y. H. Wu,[55] Y. J. Wu,[31] Z. Wu,[1,58] L. Xia,[72,58] X. M. Xian,[39] B. H. Xiang,[1,64] T. Xiang,[46,h] D. Xiao,[38,k,l] G. Y. Xiao,[42] S. Y. Xiao,[1] Y. L. Xiao,[12,g] Z. J. Xiao,[41] C. Xie,[42] X. H. Xie,[46,h] Y. Xie,[50] Y. G. Xie,[1,58] Y. H. Xie,[6] Z. P. Xie,[72,58] T. Y. Xing,[1,64] C. F. Xu,[1,64] C. J. Xu,[59] G. F. Xu,[1] H. Y. Xu,[67,2,p] M. Xu,[72,58] Q. J. Xu,[16] Q. N. Xu,[30] W. Xu,[1] W. L. Xu,[67] X. P. Xu,[55] Y. Xu,[40] Y. C. Xu,[78] Z. S. Xu,[64] F. Yan,[12,g] L. Yan,[12,g] W. B. Yan,[72,58] W. C. Yan,[81] X. Q. Yan,[1,64] H. J. Yang,[51,f] H. L. Yang,[34] H. X. Yang,[1] T. Yang,[1] Y. Yang,[12,g] Y. F. Yang,[43] Y. F. Yang,[1,64] Y. X. Yang,[1,64] Z. W. Yang,[38,k,l] Z. P. Yao,[50] M. Ye,[1,58] M. H. Ye,[8] J. H. Yin,[1] Junhao Yin,[43] Z. Y. You,[59] B. X. Yu,[1,58,64] C. X. Yu,[43] G. Yu,[1,64] J. S. Yu,[25,i] M. C. Yu,[40] T. Yu,[73] X. D. Yu,[46,h] Y. C. Yu,[81] C. Z. Yuan,[1,64] J. Yuan,[34] J. Yuan,[45] L. Yuan,[2] S. C. Yuan,[1,64] Y. Yuan,[1,64] Z. Y. Yuan,[59] C. X. Yue,[39] A. A. Zafar,[74] F. R. Zeng,[50] S. H. Zeng,[63] X. Zeng,[12,g] Y. Zeng,[25,i] Y. J. Zeng,[1,64] Y. J. Zeng,[59] X. Y. Zhai,[34] Y. C. Zhai,[50] Y. H. Zhan,[59] A. Q. Zhang,[1,64] B. L. Zhang,[1,64] B. X. Zhang,[1] D. H. Zhang,[43] G. Y. Zhang,[19] H. Zhang,[81] H. Zhang,[72,58] H. C. Zhang,[1,58,64] H. H. Zhang,[34] H. H. Zhang,[59] H. Q. Zhang,[1,58,64] H. R. Zhang,[72,58] H. Y. Zhang,[1,58] J. Zhang,[81] J. Zhang,[59] J. J. Zhang,[52] J. L. Zhang,[20] J. Q. Zhang,[41] J. S. Zhang,[12,g] J. W. Zhang,[1,58,64] J. X. Zhang,[38,k,l] J. Y. Zhang,[1] J. Z. Zhang,[1,64] Jianyu Zhang,[64] L. M. Zhang,[61] Lei Zhang,[42] P. Zhang,[1,64] Q. Y. Zhang,[34] R. Y. Zhang,[38,k,l] S. H. Zhang,[1,64] Shulei Zhang,[25,i] X. M. Zhang,[1] X. Y. Zhang,[40] X. Y. Zhang,[50] Y. Zhang,[73] Y. Zhang,[1] Y. T. Zhang,[81] Y. H. Zhang,[1,58] Y. M. Zhang,[39] Yan Zhang,[72,58] Z. D. Zhang,[1] Z. H. Zhang,[1] Z. L. Zhang,[34] Z. Y. Zhang,[43] Z. Y. Zhang,[77] Z. Z. Zhang,[45] G. Zhao,[1] J. Y. Zhao,[1,64] J. Z. Zhao,[1,58] L. Zhao,[1] Lei Zhao,[72,58] M. G. Zhao,[43] N. Zhao,[79] R. P. Zhao,[64] S. J. Zhao,[81] Y. B. Zhao,[1,58] Y. X. Zhao,[31,64] Z. G. Zhao,[72,58] A. Zhemchugov,[36,b] B. Zheng,[73] B. M. Zheng,[34] J. P. Zheng,[1,58] W. J. Zheng,[1,64] Y. H. Zheng,[64] B. Zhong,[41] X. Zhong,[59] H. Zhou,[50] J. Y. Zhou,[34] L. P. Zhou,[1,64] S. Zhou,[6] X. Zhou,[77] X. K. Zhou,[6] X. R. Zhou,[72,58] X. Y. Zhou,[39] Y. Z. Zhou,[12,g] Z. C. Zhou,[20] A. N. Zhu,[64] J. Zhu,[43] K. Zhu,[1] K. J. Zhu,[1,58,64] K. S. Zhu,[12,g] L. Zhu,[34] L. X. Zhu,[64] S. H. Zhu,[71] T. J. Zhu,[12,g] W. D. Zhu,[41] Y. C. Zhu,[72,58] Z. A. Zhu,[1,64] J. H. Zou,[1] and J. Zu[72,58]

(BESIII Collaboration)

[1]*Institute of High Energy Physics, Beijing 100049, People's Republic of China*
[2]*Beihang University, Beijing 100191, People's Republic of China*
[3]*Bochum Ruhr-University, D-44780 Bochum, Germany*
[4]*Budker Institute of Nuclear Physics SB RAS (BINP), Novosibirsk 630090, Russia*
[5]*Carnegie Mellon University, Pittsburgh, Pennsylvania 15213, USA*
[6]*Central China Normal University, Wuhan 430079, People's Republic of China*
[7]*Central South University, Changsha 410083, People's Republic of China*
[8]*China Center of Advanced Science and Technology, Beijing 100190, People's Republic of China*
[9]*China University of Geosciences, Wuhan 430074, People's Republic of China*
[10]*Chung-Ang University, Seoul, 06974, Republic of Korea*

[11]COMSATS University Islamabad, Lahore Campus, Defence Road, Off Raiwind Road, 54000 Lahore, Pakistan
[12]Fudan University, Shanghai 200433, People's Republic of China
[13]GSI Helmholtzcentre for Heavy Ion Research GmbH, D-64291 Darmstadt, Germany
[14]Guangxi Normal University, Guilin 541004, People's Republic of China
[15]Guangxi University, Nanning 530004, People's Republic of China
[16]Hangzhou Normal University, Hangzhou 310036, People's Republic of China
[17]Hebei University, Baoding 071002, People's Republic of China
[18]Helmholtz Institute Mainz, Staudinger Weg 18, D-55099 Mainz, Germany
[19]Henan Normal University, Xinxiang 453007, People's Republic of China
[20]Henan University, Kaifeng 475004, People's Republic of China
[21]Henan University of Science and Technology, Luoyang 471003, People's Republic of China
[22]Henan University of Technology, Zhengzhou 450001, People's Republic of China
[23]Huangshan College, Huangshan 245000, People's Republic of China
[24]Hunan Normal University, Changsha 410081, People's Republic of China
[25]Hunan University, Changsha 410082, People's Republic of China
[26]Indian Institute of Technology Madras, Chennai 600036, India
[27]Indiana University, Bloomington, Indiana 47405, USA
[28a]INFN Laboratori Nazionali di Frascati, I-00044, Frascati, Italy
[28b]INFN Sezione di Perugia, I-06100, Perugia, Italy
[28c]University of Perugia, I-06100, Perugia, Italy
[29a]INFN Sezione di Ferrara, I-44122, Ferrara, Italy
[29b]University of Ferrara, I-44122, Ferrara, Italy
[30]Inner Mongolia University, Hohhot 010021, People's Republic of China
[31]Institute of Modern Physics, Lanzhou 730000, People's Republic of China
[32]Institute of Physics and Technology, Peace Avenue 54B, Ulaanbaatar 13330, Mongolia
[33]Instituto de Alta Investigación, Universidad de Tarapacá, Casilla 7D, Arica 1000000, Chile
[34]Jilin University, Changchun 130012, People's Republic of China
[35]Johannes Gutenberg University of Mainz, Johann-Joachim-Becher-Weg 45, D-55099 Mainz, Germany
[36]Joint Institute for Nuclear Research, 141980 Dubna, Moscow region, Russia
[37]Justus-Liebig-Universitaet Giessen, II. Physikalisches Institut, Heinrich-Buff-Ring 16, D-35392 Giessen, Germany
[38]Lanzhou University, Lanzhou 730000, People's Republic of China
[39]Liaoning Normal University, Dalian 116029, People's Republic of China
[40]Liaoning University, Shenyang 110036, People's Republic of China
[41]Nanjing Normal University, Nanjing 210023, People's Republic of China
[42]Nanjing University, Nanjing 210093, People's Republic of China
[43]Nankai University, Tianjin 300071, People's Republic of China
[44]National Centre for Nuclear Research, Warsaw 02-093, Poland
[45]North China Electric Power University, Beijing 102206, People's Republic of China
[46]Peking University, Beijing 100871, People's Republic of China
[47]Qufu Normal University, Qufu 273165, People's Republic of China
[48]Renmin University of China, Beijing 100872, People's Republic of China
[49]Shandong Normal University, Jinan 250014, People's Republic of China
[50]Shandong University, Jinan 250100, People's Republic of China
[51]Shanghai Jiao Tong University, Shanghai 200240, People's Republic of China
[52]Shanxi Normal University, Linfen 041004, People's Republic of China
[53]Shanxi University, Taiyuan 030006, People's Republic of China
[54]Sichuan University, Chengdu 610064, People's Republic of China
[55]Soochow University, Suzhou 215006, People's Republic of China
[56]South China Normal University, Guangzhou 510006, People's Republic of China
[57]Southeast University, Nanjing 211100, People's Republic of China
[58]State Key Laboratory of Particle Detection and Electronics, Beijing 100049, Hefei 230026, People's Republic of China
[59]Sun Yat-Sen University, Guangzhou 510275, People's Republic of China
[60]Suranaree University of Technology, University Avenue 111, Nakhon Ratchasima 30000, Thailand
[61]Tsinghua University, Beijing 100084, People's Republic of China
[62a]Turkish Accelerator Center Particle Factory Group, Istinye University, 34010, Istanbul, Turkey
[62b]Near East University, Nicosia, North Cyprus, 99138, Mersin 10, Turkey
[63]University of Bristol, H H Wills Physics Laboratory, Tyndall Avenue, Bristol BS8 1TL, United Kingdom

[64]*University of Chinese Academy of Sciences, Beijing 100049, People's Republic of China*
[65]*University of Groningen, NL-9747 AA Groningen, The Netherlands*
[66]*University of Hawaii, Honolulu, Hawaii 96822, USA*
[67]*University of Jinan, Jinan 250022, People's Republic of China*
[68]*University of Manchester, Oxford Road, Manchester, M13 9PL, United Kingdom*
[69]*University of Muenster, Wilhelm-Klemm-Strasse 9, 48149 Muenster, Germany*
[70]*University of Oxford, Keble Road, Oxford OX13RH, United Kingdom*
[71]*University of Science and Technology Liaoning, Anshan 114051, People's Republic of China*
[72]*University of Science and Technology of China, Hefei 230026, People's Republic of China*
[73]*University of South China, Hengyang 421001, People's Republic of China*
[74]*University of the Punjab, Lahore-54590, Pakistan*
[75a]*University of Turin and INFN, I-10125, Turin, Italy*
[75b]*University of Eastern Piedmont, I-15121, Alessandria, Italy*
[75c]*INFN, I-10125, Turin, Italy*
[76]*Uppsala University, Box 516, SE-75120 Uppsala, Sweden*
[77]*Wuhan University, Wuhan 430072, People's Republic of China*
[78]*Yantai University, Yantai 264005, People's Republic of China*
[79]*Yunnan University, Kunming 650500, People's Republic of China*
[80]*Zhejiang University, Hangzhou 310027, People's Republic of China*
[81]*Zhengzhou University, Zhengzhou 450001, People's Republic of China*

[a]Deceased.
[b]Also at the Moscow Institute of Physics and Technology, Moscow 141700, Russia.
[c]Also at the Novosibirsk State University, Novosibirsk, 630090, Russia.
[d]Also at the NRC "Kurchatov Institute," PNPI, 188300, Gatchina, Russia.
[e]Also at Goethe University Frankfurt, 60323 Frankfurt am Main, Germany.
[f]Also at Key Laboratory for Particle Physics, Astrophysics and Cosmology, Ministry of Education; Shanghai Key Laboratory for Particle Physics and Cosmology; Institute of Nuclear and Particle Physics, Shanghai 200240, People's Republic of China.
[g]Also at Key Laboratory of Nuclear Physics and Ion-beam Application (MOE) and Institute of Modern Physics, Fudan University, Shanghai 200443, People's Republic of China.
[h]Also at State Key Laboratory of Nuclear Physics and Technology, Peking University, Beijing 100871, People's Republic of China.
[i]Also at School of Physics and Electronics, Hunan University, Changsha 410082, China.
[j]Also at Guangdong Provincial Key Laboratory of Nuclear Science, Institute of Quantum Matter, South China Normal University, Guangzhou 510006, China.
[k]Also at MOE Frontiers Science Center for Rare Isotopes, Lanzhou University, Lanzhou 730000, People's Republic of China.
[l]Also at Lanzhou Center for Theoretical Physics, Lanzhou University, Lanzhou 730000, People's Republic of China.
[m]Also at the Department of Mathematical Sciences, IBA, Karachi 75270, Pakistan.
[n]Also at Ecole Polytechnique Federale de Lausanne (EPFL), CH-1015 Lausanne, Switzerland.
[o]Also at Helmholtz Institute Mainz, Staudinger Weg 18, D-55099 Mainz, Germany.
[p]Also at School of Physics, Beihang University, Beijing 100191, China.